



Evidence for deep-water deposition of abyssal Mediterranean evaporites during the Messinian salinity crisis



Elizabeth C. Christeleit^{a,*}, Mark T. Brandon^a, Guangsheng Zhuang^{a,b}

^a Department of Geology and Geophysics, Yale University, P.O. Box 208109, New Haven, CT 06520-8109, United States

^b Lancaster Environment Centre, Lancaster University, LA1 4YQ, Lancaster, United Kingdom

ARTICLE INFO

Article history:

Received 24 March 2015

Received in revised form 28 June 2015

Accepted 29 June 2015

Available online 24 July 2015

Editor: D. Vance

Keywords:

Messinian salinity crisis

ACE index

TEX₈₆

Mediterranean sea

deep sea drilling project

ABSTRACT

Scientific drilling of the abyssal evaporites beneath the deepest parts of the Mediterranean basin gave rise to the idea that the Mediterranean sea completely evaporated at the end of the Messinian. Herein, we show, using new organic geochemical data, that those evaporites were deposited beneath a deep-water saline basin, not in a subaerial saltpan, as originally proposed. Abundant fossil organic lipids were extracted from evaporites in Mediterranean Deep Sea Drilling Project cores. The archaeal lipid distribution and new analyses, using the ACE salinity proxy and TEX₈₆ temperature proxy, indicate that surface waters at the time of evaporite deposition had normal marine salinity, ranging from ~26 to 34 practical salinity units, and temperatures of 25–28 °C. These conditions require a deep-water setting, with a mixed layer with normal marine salinity and an underlying brine layer at gypsum and halite saturation. After correction for isostatic rebound, our results indicate maximum drawdown of ~2000 m and ~2900 m relative to modern sea level in the western and eastern Mediterranean basins, respectively. Our results are consistent with previously proposed scenarios for sea level drawdown based on both subaerial and submarine incision and backfilling of the Rhone and Nile rivers, which require Messinian sea level drops of ~1300 m and ~200 m, respectively. This study provides new evidence for an old debate and also demonstrates the importance of further scientific drilling and sampling of deeper part of the abyssal Messinian units.

© 2015 Elsevier B.V. All rights reserved.

1. Introduction

Field studies dating back to the 1860s and renewed study in the 1950s of Late Miocene evaporites exposed around the margin of the Mediterranean provided the first evidence of widespread drawdown of the Mediterranean at about 6 Ma (Mottura, 1872; Ogniben, 1957). Seismic reflection profiling in the late 1960s revealed that the abyssal basins of the Mediterranean, such as the Sardinio-Balearic basin in the western Mediterranean (~2850 mbsl, meters below modern sea level), the Ionian basin in the central Mediterranean (~4100 mbsl), and the Herodotus basin in the eastern Mediterranean (~3000 mbsl), are also underlain by extensive Messinian-age evaporites, some 1 to 2 km thick (for details about this early history, see Ryan, 2009). These abyssal Messinian deposits were first sampled by deep-sea drilling in 1970 (Ryan et al., 1973a, 1973b; Hsü et al., 1978). That work gave rise to the surprising idea that the Mediterranean Sea may have fully evaporated during the Messinian salinity crisis, leaving behind a vast desert landscape ~2 to 4 km below global sea level (Hsü, 1972; Hsü et

al., 1973a, 1973b). This hypothesis, based partially on sedimentological features in the abyssal evaporites, has been hotly debated (e.g. Hardie and Lowenstein, 2004), but remains an enduring idea of the Messinian salinity crisis.

The Messinian salinity crisis is now precisely dated to 5.97 to 5.33 Ma (Krijgsman et al., 1999; Manzi et al., 2013). Drilling and seismic profiling have demonstrated deep incision and subsequent backfilling of the lower reaches of the Nile and Rhone rivers during the Messinian salinity crisis (Barber, 1981; Clauzon, 1982). Seismic profiling has also revealed an erosional unconformity around the higher parts of the Mediterranean, and reworking of evaporite detritus into the lower parts of the basin (e.g. Lofi et al., 2011). Hydrologic (Debenedetti, 1982; Blanc, 2006; Meijer and Krijgsman, 2005) and isostatic (Norman and Chase, 1986; Govers et al., 2009) modeling have helped clarify the response of the basin to changing climate, water supply, and sediment and water loads. These studies, and many others (see reviews by Ryan, 2009 and Roveri et al., 2014a), have aided our understanding of the Messinian salinity crisis. For example, in the original “shallow-water deep-basin” hypothesis, Hsü and colleagues (Hsü, 1972; Hsü et al., 1973a, 1973b) used the term “desiccated deep basin” to refer to a Mediterranean that was completely evaporated. Subsequent

* Corresponding author.

E-mail address: elizabeth.christeleit@yale.edu (E.C. Christeleit).

papers have refined this desiccation hypothesis and stretched the terminology to include various scenarios involving only partial evaporation of the Mediterranean (e.g. Meijer and Krijgsman, 2005; Ryan, 2009). There has also been much important work on the marginal Messinian, but those deposits formed in relative high positions within the basin and thus provide little direct evidence about the depositional setting of the deep Mediterranean basins. Apart from deep-sea cores, there is no direct evidence for the depositional environment of the abyssal Messinian evaporites.

Around the same time as the discovery of the Messinian salinity crisis, there was an active debate about the origin of “saline giants”, which are massive evaporite deposits seen throughout the geologic record. It was well established that halite and gypsum could be deposited in deep-water silled basin, given the appropriate climatic constraints and basin geometry (e.g. Schmalz, 1969; Brongersma-Sanders, 1971). In this sense, “deep” refers to a water depth where storm waves cannot reach the bottom of the basin. For brine-filled basins, this transition occurs at about 50 m (Sonnenfeld, 1985). Several papers propose credible deep-water interpretations for the Messinian salinity crisis (Brongersma-Sanders, 1971; Debenedetti, 1982; Schmalz, 1991), but those ideas have been commonly discounted, mainly because there is no modern analogue for deep-water evaporite deposition (Hsü, 1972). It should be noted that there is also no modern analogue for a fully evaporated abyssal basin.

In the debate about the Messinian salinity crisis, what has been lacking is way to estimate the amount of evaporative drawdown of the deep Mediterranean basins during the deposition of the abyssal evaporites. This question cannot be addressed by studies of deposition and erosion in marginal settings. Instead, the key to this problem is determining the depositional environment of the abyssal evaporites. Our approach is to use organic geochemistry to estimate key paleoenvironmental indicators for the available core samples of abyssal evaporites. Relative abundances of fossil archaeal lipids are commonly used to determine the paleoenvironment of sediments, including temperature and salinity (Schouten et al., 2002; Turich and Freeman, 2011). Here we use this analysis to characterize the evaporite facies of the abyssal Mediterranean at the end of the Messinian, and provide an upper limit for the amount of sea level drawdown. We also integrate our new data with proposed scenarios for the Messinian salinity crisis by discussing other constraints on water depth.

2. Materials and methods

2.1. Sample locations

Samples of anhydrite, halite, and gypsum from three drill sites in the Sardinian-Balearic and Ionian abyssal basins (Fig. 1) were obtained from the International Core Repository at the University of Bremen. The sites are in abyssal settings, 35–200 km from adjacent continental margins, located at modern water depths of 2.5–4 km.

The abyssal Messinian deposits are 1–2 km thick and are typically divided, on the basis of seismic reflection data, into the Lower Unit, middle Mobile Unit, and Upper Unit (Lofi et al., 2011; Roveri et al., 2014c). The Lower Unit is stratified, but the Mobile Unit shows extensive diapirism, which suggests it is dominated by halite. It is important to note that drilling has sampled no deeper than 160 m into the upper part of the abyssal Messinian evaporites, which amounts to only ~10% of the section (Ryan et al., 1973a, 1973b; Hsü et al., 1978). Thus, our conclusions here are limited to the uppermost part of the abyssal Messinian evaporites. While there has been much speculation about deeper parts of the abyssal Messinian deposits, at present there are no samples from that part of the section.

Leg 42A Site 374 has a seafloor depth of 4088 m and is located in the eastern Mediterranean basin, 200 km east of the Malta Escarpment and 300 km from the European and African continents (Fig. 1). The evaporites are overlain by 373 m of Pleistocene and Pliocene nanofossil ooze, typical of an open-marine environment, with thin layers of siliciclastic silt, interpreted as distal turbidites (Hsü et al., 1978). The cored portion of the underlying Messinian contains alternating layers of dolomitic mudstone with gypsum crystals, and fine wavy laminae of gypsum and anhydrite (Figs. 2A and 2B).

Leg 13 Site 134 has a seafloor depth of 2864 m and is located at the base of the Sardinian continental slope (Fig. 1). The top 344 m of the drilled section consists of Quaternary and Pliocene nanofossil ooze, with minor pebbles and gravel of terrigenous material (Ryan et al., 1973b). The cored Messinian interval is composed mostly of halite with small anhydrite nodules (Fig. 2C) and thin silty layers with a minor component (<10%) of siliciclastic sediment, attributed to a windblown source (Hsü et al., 1973c).

Leg 13 Site 124 has a sea floor depth of 2726 m and is located in the western Sardinian-Balearic abyssal plain, 300 km west of Sardinia and over 500 km from the Gulf of Lion, where the Rhone River empties into the Mediterranean (Fig. 1). The top 359 m of the drilled section consists of Quaternary and Pliocene nanofossil ooze, marls and sands (Ryan et al., 1973a). The cored Messinian interval contains abundant anhydrite nodules, up to 3 cm in diameter, with thin veins of carbonate and mud (Fig. 2D).

The evaporative textures in the cores deposits are not diagnostic of a particular depositional environment or water depth. For example, the shipboard scientists (Hsü et al., 1978) interpreted laminae in the dolomitic mudstone (site 374) as photic zone algal stromatolites, which would be diagnostic of a shallow-water setting. Hardie and Lowenstein (2004) note that wavy laminae are also formed in deep-water settings. The “hopper texture” of halite (site 134) was thought to be indicative of subaerial deposition (Hsü et al., 1973c). Hardie and Lowenstein (2004) and Roveri et al. (2014b) dispute this interpretation. Other early work argues that the similarity of anhydrite deposits (site 124) to “chicken-wire” anhydrite texture found in modern subaerial coastal salt flats (sabkhas) in the Persian Gulf is diagnostic of a subaerial setting (Hsü, 1972). Others suggest that nodular anhydrite is not diagnostic of subaerial deposition (Schreiber and El Tabakh, 2000; Hardie and Lowenstein, 2004).

2.2. Sample preparation and analysis

Organic compounds, including cell-membrane lipids of Archaea, were extracted and analyzed using standard procedures following Schouten et al. (2007). Samples were manually crushed, freeze dried for >48 h, and stored at -21°C . Dry samples were then powdered and extracted using an accelerated solvent extractor (Dionex-ASE 300) with dichloromethane/methanol solution (2:1, by volume). Total lipid extracts were concentrated using a solvent evaporator (Zymark Turbovap II) and then dried under a stream of purified N_2 . Silica-gel chromatography was then used to separate the lipid extract into compound-specific fractions. Ashed Pasteur pipettes loaded with approximately 0.5 g deactivated silica gel (70–230 mesh) were sequentially eluted with 4 ml hexane, 4 ml dichloromethane, and 4 ml of methanol to obtain aliphatic, aromatic, and polar fractions, respectively. The polar fraction, which contains diethers and tetraethers, was filtered through 0.7 μm glass microfiber filter, then dried under pure N_2 stream, and then loaded into a solution of hexane/isopropanol (99:1, by volume).

Extracted samples were analyzed on a high-performance liquid-chromatography atmospheric-pressure chemical-ionization mass spectrometer (Agilent 1200 Series HPLC-APCI-MS, equipped with automatic injector and HP Chemstation software). Liquid

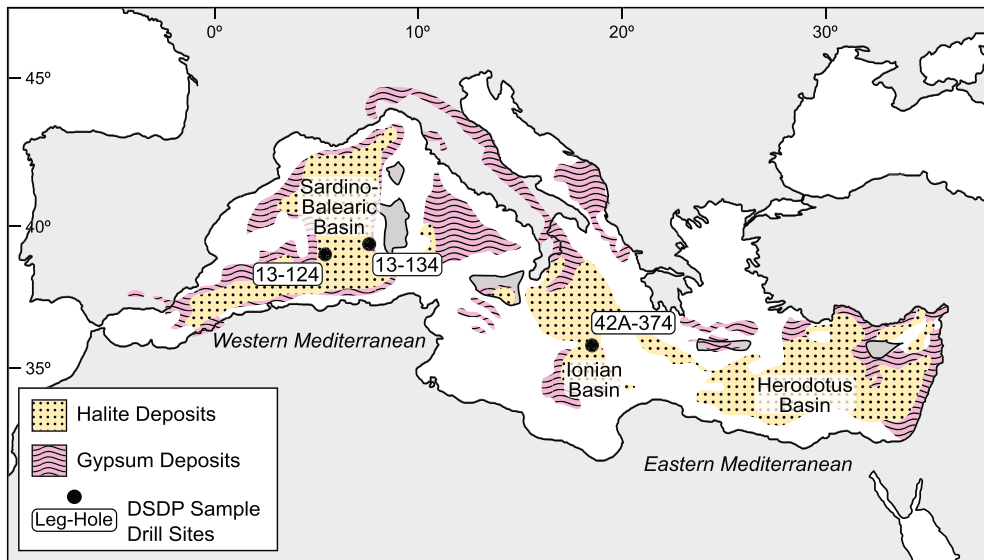


Fig. 1. Extent of abyssal and marginal Messinian evaporites in the Mediterranean region and locations of 3 DSDP sites in the Sardino-Balearic and Ionian Abyssal basins.

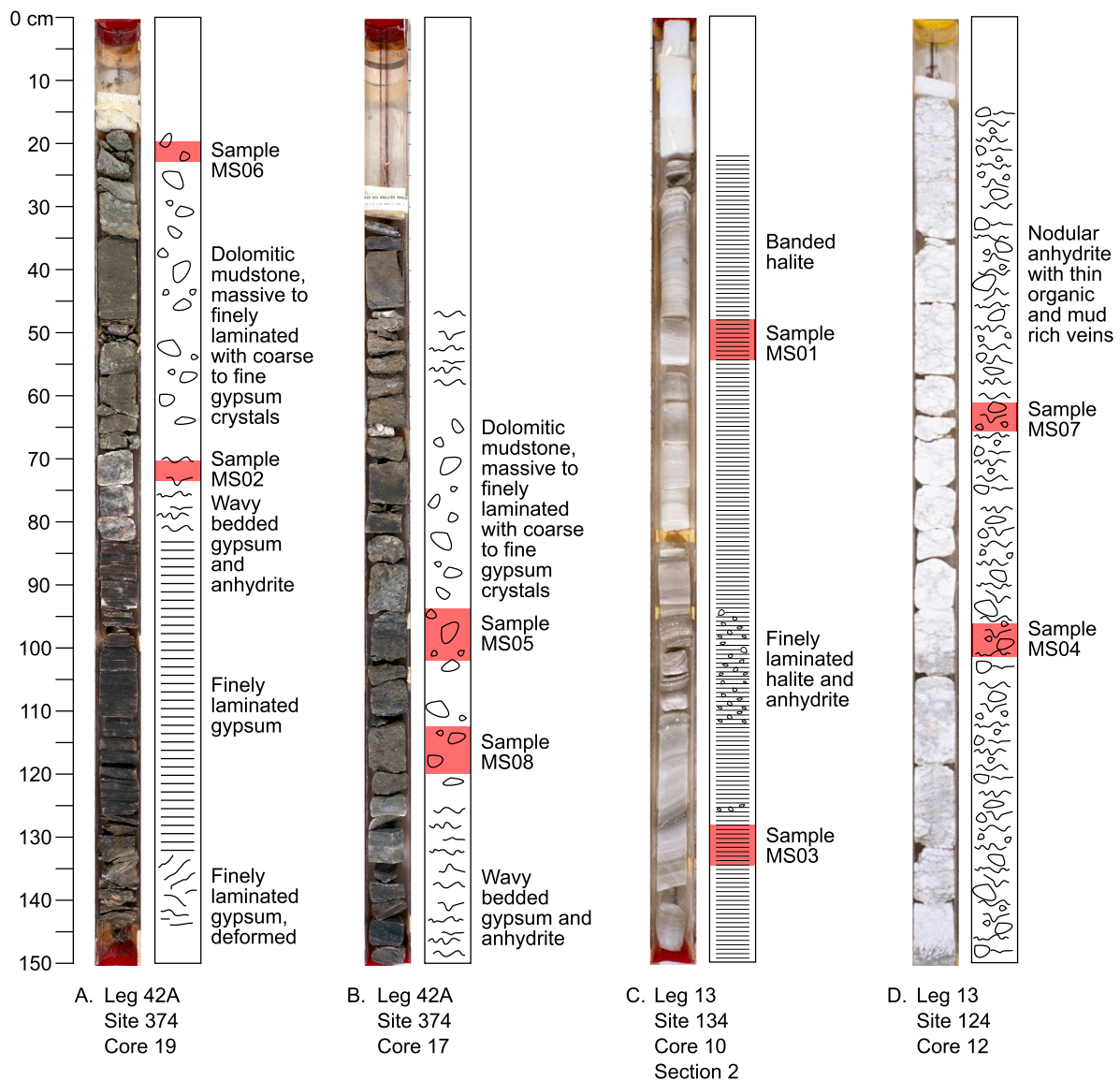


Fig. 2. Core images, visual descriptions, and locations of each sample. Core images are from the Integrated Ocean Drilling Program Core Photo database. See text for explanation.

chromatography was done using a Prevail Cyano column (2.1 × 150 mm, 3 μm; Alltech, Deerfield, IL). The mobile-phase solvent A (hexane/isopropanol 99:1, by volume) was added at 0.2 ml/min isocratically for 5 min, followed by introduction of solvent B (hexane/isopropanol 90:10, by volume) that increased linearly from 0% at 5 min to 7.4% at 40 min, and then held steady for 10 min. The column was cleaned with 100% solvent B for 14 min in back-flush mode, followed by 10 min equilibration with 100% solvent A. Archaeol and tetraethers were measured on the mass spectrometer using scans for single ions $[M + H]^+$. Concentrations were determined by integrating relevant single-ion peaks determined by comparison with an external lab standard. Relative abundances of specific membrane lipids were used to calculate the paleoenvironment indicators described in detail below.

3. Paleoenvironment indicators

3.1. Lipid biomarkers

Dense communities of halotolerant and halophilic organisms, including a variety of Archaea, bacteria, and eukaryotes, thrive in modern hypersaline environments. Previous paleobiology studies find ample evidence that halophilic microorganisms were present in the water column during deposition of the marginal Messinian evaporites (e.g. Turich and Freeman, 2011; Birgel et al., 2014). Our study is the first to use modern methods to isolate molecular organic compounds that are diagnostic of the environmental setting of the uppermost abyssal Messinian evaporites.

We find that 7 of the 8 abyssal evaporite samples contain abundant remains of lipids derived from cell membranes of microorganisms of the domain Archaea. Diagnostic core lipids of Archaea are known to remain intact in sedimentary deposits for periods up to 100 Ma, as long as temperatures remain less than 240 °C (see Schouten et al., 2013 and references within). Our samples are buried no deeper than 420 m, so temperatures were never high enough to degrade the relevant lipids. The lipid compounds present in the samples include glycerol dialkyl glycerol tetraethers (GDGTs), including acyclic caldarchaeol (GDGT-0) and cyclic crenarchaeol (GDGT-5), as well as archaeol diethers. Various groups of Archaea produce one or all of these types of compounds. Halophilic forms of Archaea appear to only produce diether lipids, including archaeol, whereas marine Archaea produce diether lipids, caldarchaeol and cyclic GDGTs (Schouten et al., 2013, and references within). Marine Crenarchaeota were originally the only form of Archaea known to produce crenarchaeol (Sinninghe Damsté et al., 2002), and this compound was proposed as a biomarker for this group of Archaea (Schouten et al., 2002; Sinninghe Damsté et al., 2002; Pearson and Ingalls, 2013). Further study has shown that crenarchaeol is also synthesized by thermophilic Archaea (Schouten et al., 2013, and references within).

Investigations in modern settings document how the relative abundances of archaeal lipids vary throughout the water column and across extreme temperature and salinity gradients (Karner et al., 2001; Schouten et al., 2002; Turich et al., 2007; Turich and Freeman, 2011). Relative abundances of archaeal lipids form the basis for estimating sea-surface temperature (Schouten et al., 2002), and salinity (Turich and Freeman, 2011), discussed in detail below. To a first order, the presence or absence of particular lipids can be indicative of a particular environmental setting. For example, our samples contain relative abundances of GDGTs, including crenarchaeol, which are typical of open marine environments (Sinninghe Damsté et al., 2002; Turich et al., 2007; Turich and Freeman, 2011). This is in contrast to hypersaline environments, which are dominated by halophilic Archaea, and thus tend to have higher relative abundances of archaeol and caldarchaeol, and low abundances of crenarchaeol (Turich et al., 2007).

3.2. TEX₈₆ paleotemperature proxy

Schouten et al. (2002) introduce the TEX₈₆ index (TetraEther index consisting of 86 carbons), which is defined by the relative abundances of a set of tetraether compounds that are sensitive to water temperature (see reviews Schouten et al., 2013; Pearson and Ingalls, 2013). Archaea that synthesize GDGT compounds live throughout the water column, but thrive at the base of the photic zone and in subphotic waters (Karner et al., 2001; Pearson and Ingalls, 2013). The TEX₈₆ index appears to work best at predicting sea-surface temperature (Schouten et al., 2002; Liu et al., 2009; Kim et al., 2010). This result may seem odd, given that Archaea abundances commonly peak below this range of depths. Schouten et al. (2013) note that archaeal cell debris is too small and too buoyant to sink by itself through the water column. Some intermediate process—such as packaging in fecal pellets or adsorption onto mineral grains—is needed to account for the accumulation of GDGT compounds in sea-floor sediments, and that intermediate process may be biased towards Archaea that live in the top of the water column.

We use the TEX₈₆ temperature proxy to discriminate between high surface temperatures characteristic of shallow brine pools, and more moderate surface temperatures characteristic of deep stratified saline bodies. Our results are reported in Table 1 and Fig. 3A. There are several calibrations for the TEX₈₆ proxy (see Schouten et al., 2013 and references within). In this study, we use the calibration of Liu et al. (2009), where $T(C) = -16.3 * (1/TEX_{86}) + 50.5$. This calibration works well over a range of settings, including high-temperature surface waters of the Red Sea, which is a potential modern analogue for the Messinian Mediterranean. For comparison, Fig. 3A also shows estimates using the Kim et al. (2010) TEX₈₆^H calibration.

Our TEX₈₆ measurements show little variation, from 0.65 and 0.72, corresponding to temperatures between 25–28 °C. There is little difference between estimates based on the Liu et al. (2009) and Kim et al. (2010) calibrations. The TEX₈₆ values are well within the range of data used in the proxy calibrations and are lower than values seen in modern high-salinity, high-temperature environments like the Red Sea (Trommer et al., 2009). Studies in both laboratory and natural settings have found that salinity does not affect the TEX₈₆ proxy (Trommer et al., 2009; Wuchter et al., 2004). There is active debate about whether TEX₈₆ temperatures reflect annual average sea-surface temperatures, or seasonal sea-surface temperatures (Pearson and Ingalls, 2013). The basin-wide average temperature of the modern Mediterranean surface layer is 14.4 °C in February and 24.9 °C in August (Houpert et al., 2015). Our Miocene TEX₈₆ temperatures of 25–28 °C are warmer than any month for the modern Mediterranean, which may reflect a warmer Miocene climate.

3.3. ACE index for paleosalinity

Distinct groups of Archaea have different salinity tolerances, from fresh to hypersaline waters. These archaeal groups are distinguished by the lipids they produce; halophilic forms of Archaea appear to produce the diether archaeol, whereas marine Euryarchaeota produce tetraethers, including the acyclic compound caldarchaeol (Turich et al., 2007). Turich and Freeman (2011) introduce an index called ACE (archaeol and caldarchaeol ecometric) based on the relative abundance of these two lipid compounds. They show that the index has a strong correlation with salinity in modern settings (Fig. 3B).

The HPLC-APCI-MS instrumentation allows for archaeol and caldarchaeol abundances in a sample to be estimated in a single analysis. The ACE index is then calculated using,

Table 1
Core sample locations, descriptions, and organic geochemistry results. LIS01 and LIS02 are in-house laboratory standards from Long Island Sound with known salinity of ~26 psu. No archaeal lipids were detected in sample MS03. All salinity estimates have a 95% prediction interval of ± 27 psu.

Sample	Rock type	Leg-site-core-section	BIT index	ACE index	Salinity (psu)	TEX ₈₆ (°C)	Temperature (°C)
MS06	Gypsum in mudstone	42A-374-19-1	0.15	3.1	34	0.72	28
MS02	Bedded gypsum and anhydrite	42A-374-19-2	0.30	1.9	30	0.65	25
MS05	Gypsum in mudstone	42A-374-17-1	0.09	0.3	26	0.71	28
MS08	Gypsum in mudstone	42A-374-17-2	0.11	0.7	27	0.66	26
MS01	Laminated halite	13-134-10-1	0.25	0.8	28	0.65	25
MS03	Laminated halite	13-134-10-2	–	–	–	–	–
MS07	Nodular anhydrite	13-124-12-2	0.02	1.1	28	0.65	26
MS04	Nodular anhydrite	13-124-12-1	0.06	2.7	33	0.67	26
LIS01	Standard	–	–	0.2	26	0.442	13.5
LIS02	Standard	–	–	0.2	26	0.443	13.6

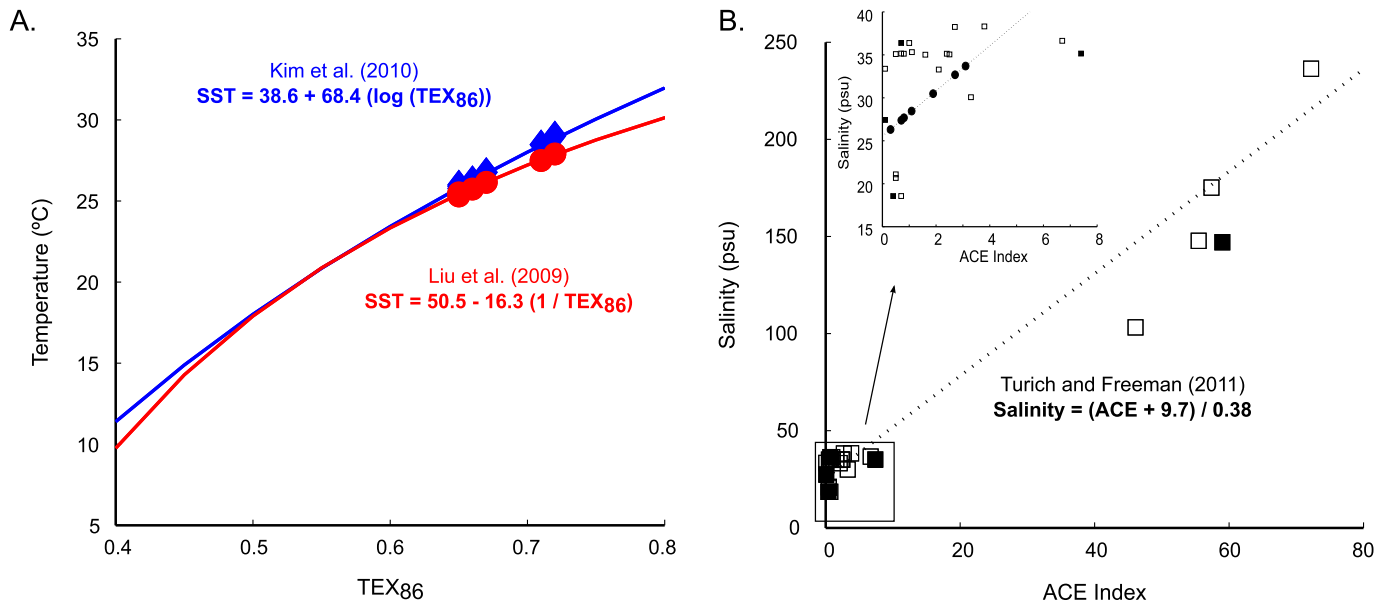


Fig. 3. Proxy calibrations used to estimate surface temperature and salinity. (A) TEX₈₆ and temperature correlations from Liu et al. (2009) (red line) and Kim et al. (2010) (blue line). Solid circles and diamonds are the temperature estimates for this study using the respective calibrations. (B) ACE index and salinity correlation from Turich and Freeman (2011), where open squares are modern suspended particle matter and solid squares are modern surface sediments. The dashed line is the correlation used for our samples, given that they lack a significant terrestrial component. Solid circles in the inset plot show ACE index and salinity estimates for the abyssal Mediterranean samples. (For interpretation of the references to color in this figure, the reader is referred to the web version of this article.)

$$ACE = \frac{A_A R_{C/A}}{A_C + A_A R_{C/A}} * 100$$

where A_A and A_C are peak areas for archaeol and caldarchaeol, respectively. $R_{C/A}$ is the relative response factor $R_{C/A} = R_C/R_A$, where R_C and R_A are the absolute response factors. Using pure standards, Turich and Freeman (2011) estimate $R_{C/A} \approx 0.01$ for their measurements. They suggest that the orders of magnitude difference in their measured archaeol and caldarchaeol response factors may be due to the fact that diethers are smaller and more volatile than tetraethers, and are therefore more efficiently ionized by their APCI. Other labs report $R_{C/A}$ values of 0.1 and 0.93 (Wang et al., 2013, and Birgel et al., 2014, respectively). We use an in-house standard of known salinity to estimate the $R_{C/A} = 0.068$ for our instrumentation. This standard is from a box core of mud deposited over the last 30 years from western Long Island Sound (40.87792°N, 73.74622°W, water depth 19 m). The mean annual salinity in this location is 24–28 psu (Thomas, 2015). The estimate for $R_{C/A}$ is given by:

$$R_{C/A} = \frac{A_C}{A_A} * \frac{(ACE_{pred}/100)}{(1 - ACE_{pred}/100)}$$

where $ACE_{pred} = (Salinity * 0.38) - 9.7$ (Turich and Freeman, 2011), the predicted ACE value for the known salinity of the standard.

The ACE index is calibrated using a dataset of 26 samples with salinities ranging from ~0–250 psu (Fig. 3B). There is a strong linear relationship between the observed salinity and the relative abundances of archaeol and caldarchaeol over the entire range of the data (Fig. 3B), but there is scatter in the data at fresh and marine salinities (<~35 psu). Given the limitations of this novel proxy, Turich and Freeman (2011) recommend a conservative usage of the ACE index, with ACE <1 indicating brackish surface water (<25 psu), ACE <10 indicating normal marine surface water (<50 psu), and ACE >40 indicating hypersaline surface water (>75 psu). Our samples from the uppermost part of the abyssal Messinian deposits have ACE values ranging from 0.29 to 3, indicating marine salinities between 26 and 34 psu, with 95% confidence intervals of ± 27 psu (Table 1; Fig. 3B). For comparison, gypsum and halite require ~110 psu and ~250 psu, respectively, for precipitation. The estimated uncertainty in the absolute salinity estimates accounts for errors in the calibration, and was calculated using the classical method for calibration (Osborne, 1991). Note that the calibration has a large $R^2 = 0.95$ (Turich and Freeman, 2011), which means that there is little difference between the classical method and the inverse method (Mark and Church, 1977). Thus, even in light of the large uncertainties, our samples have predicted salinities within the range of normal seawater. A Messinian halite sample, where we expect to find the highest

salinity, gives a predicted salinity of 28 psu (95% prediction interval, 1 to 56 psu), well below the hypersaline range.

Turich and Freeman (2011) infer that the ACE index is most sensitive to the salinity of the “surface layer” (e.g. photic zone or mixed layer). There is good agreement in their ACE values for suspended particulate matter and associated bottom sediments. Wang et al. (2013) also reports paired measurements for lakes in the Qaidam Basin on the Tibetan Plateau. ACE values for lipids from lake-bottom sediments closely match those from the overlying surface waters for salinities from 0 to 308 psu. These observations support the inference made by Turich and Freeman (2011) that the ACE proxy is representative of the salinity of surface waters.

3.4. BIT index for terrestrial input

The branched and isoprenoid tetraether (BIT) index (Hopmans et al., 2004) is widely used to test for the abundance of tetraether lipids derived from terrestrial sources. Our samples have BIT values below 0.3 (Table 1), indicating open marine environments, with little terrestrial input. This result is consistent with the abyssal setting of the drilling sites and a general absence of terrigenous material in core samples from the Messinian.

4. Discussion

4.1. Implications for water depth

Our measurements provide new information about the paleoenvironment during the time of evaporite deposition. We now focus on using these data to resolve the depositional setting, whether in shallow water or deep water. Depth is a primary control on whether water bodies are well mixed or stratified. Winds at the air–water surface generate waves, which cause mixing down to wave base (Brainerd and Gregg, 1995). Thermal convection can cause further mixing, especially when the surface layer is underlain by stratified brine (Schreiber and El Tabakh, 2000). Collectively, these processes give rise to what is called the mixed layer. In the modern Sardinia-Balearic and Ionian basins, the mixed layer depth varies seasonally between ~10–75 m (Houpert et al., 2015). Storm-wave base marks the maximum depth of mixing by surface waves. For normal marine waters, storm-wave base is ~100 m, but for dense brines, storm-wave base is smaller, ~50 m (Dietz, 1963; Sonnenfeld, 1985).

Shallow-water basins are entirely above wave base, resulting in a well-mixed water column with homogeneous temperature and salinity. Shallow-water evaporitic settings include ephemeral lakes in Death Valley (e.g. Badwater Basin) and the Great Salt Lake, which have maximum depths less than 10 m. Absorption of solar radiation increases with salinity (Schreiber and El Tabakh, 2000). As a result, a shallow-water body is warmer when it is composed of hypersaline water relative to fresh or marine water. Shallow saline bodies also experience extreme diurnal and seasonal temperature variations, closely correlated with air temperature (Lowenstein et al., 1998; Crosman and Horel, 2009).

Deep-water basins have a significant volume below wave base (Sonnenfeld, 1985). In hypersaline settings, which tend to have large vertical gradients in density, the bottom water and upper mixed layer are commonly stably stratified (Brainerd and Gregg, 1995). The mixed layer in a deep-water saline body will generally have lower temperature and salinity than that in a shallow-water saline body. The closest modern analogue for deep-water evaporite deposition is the Dead Sea during meromictic periods, where the water column remains stably stratified throughout the year. Anthropogenic activity, including diversion of freshwater, has strongly affected stratification in the Dead Sea in the last few decades (Gertman and Hecht, 2002). Prior to 1978, the deep part

of the Dead Sea was supersaturated with respect to halite precipitation, while the mixed layer had relatively lower salinity because of freshwater input.

The sediments that we analyzed contain a geochemical record of relatively low surface water temperatures and marine salinity (Fig. 4). Furthermore, the high abundance of crenarchaeol indicates normal marine surface water at the time of deposition. In contrast, these sediments are composed of gypsum and halite, which can only be precipitated from high salinity waters. These key observations are only compatible with a deep-water basin. The mixed layer is able to maintain relatively low salinity and temperature, while the deep part of the basin becomes increasingly saline with increasing evaporation. While our geochemical results indicate similar surface temperature and salinity estimates in the late Messinian Sardinia-Balearic and Ionian basins, there is nothing in our data that indicates the degree of communication between these basins. Our spatial resolution is limited to a few sites, and while the samples share a similar position within the uppermost part of the abyssal Messinian, they may be somewhat different in age (Roveri et al., 2014c).

4.2. Deep-water evaporitic basin model

The deep-water interpretation (Schmalz, 1969, 1991; Brongersma-Sanders, 1971; Debenedetti, 1982) has received little consideration in the long debate about the Messinian salinity crisis (with notable exceptions, such as Govers et al., 2009; Roveri et al., 2014a, 2014b). In a widely overlooked paper, Debenedetti (1982) identifies two important feedbacks that likely prevent the full evaporation of silled deep-water basins, where the sill allows for an inflow of seawater but blocks the outflow of deeper, more saline bottom water. First, as the water level falls, the area of the evaporating surface decreases, lowering the net evaporation from the basin. Second, theoretical and experimental studies show that evaporation rate varies inversely with salinity (e.g. Salhotra et al., 1985). As the brine becomes more concentrated, the saturation vapor pressure at the surface decreases, reducing the evaporation rate (Debenedetti, 1982; Salhotra et al., 1985). Given these feedbacks, the water level in the basin will reach an equilibrium water level where the evaporative outflux is balanced by the influx of seawater over the sill and fresh water runoff from surrounding continental regions (Debenedetti, 1982).

Oceanographic studies (Blanc, 2006; Meijer and Krijgsman, 2005) have explored how the Mediterranean equilibrium water level is influenced by variations in influx of seawater and runoff, and outflux by evaporation. These models represent the Messinian salinity crisis by maintaining modern influxes of riverine water and precipitation, and modern evaporation rates, but otherwise blocking the outflux of saline water at the Straits of Gibraltar. Meijer and Krijgsman (2005) use a Miocene reconstruction of the Mediterranean bathymetry to estimate equilibrium water level of 2515 mbsl and 2725 mbsl for the western and eastern sub-basins of the Mediterranean. They do not account for influence of salinity on evaporation rate, so their estimates of equilibrium water levels are probably too deep. Nevertheless, the analysis shows that even without this negative feedback on evaporation rate, the eastern and western Mediterranean basins were not completely evaporated. More recent modeling by Topper and Meijer (2013) includes the effect of salinity in evaporations, but the Meijer and Krijgsman (2005) analysis has not yet been updated to account for this effect.

4.3. Water depth constraints from marginal Messinian deposits

Our results provide a water depth constraint during the time of deposition of the uppermost abyssal Messinian evaporites. Others have estimated Messinian drawdown based on channel incision

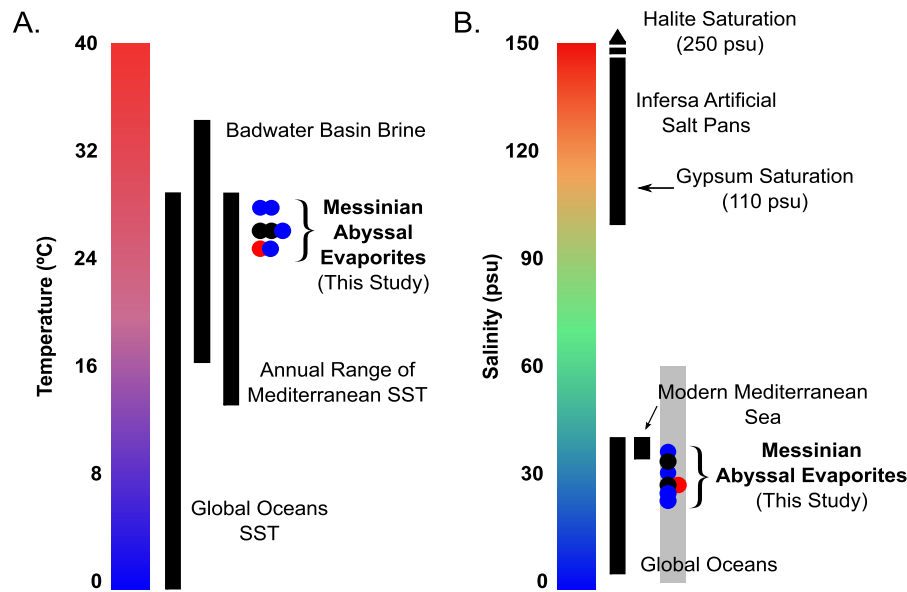


Fig. 4. Temperature and salinity estimates for our samples of the uppermost abyssal Messinian evaporites. The color of the circles indicates the main evaporite phase in each sample: blue = gypsum, black = anhydrite, and red = halite. (A) Estimates of the surface temperature fall in a narrow range (25–28 °C). For comparison, also shown are the range of winter and summer sea-surface temperatures (SST) of the modern Mediterranean Sea (14.4–24.9 °C; Houpert et al., 2015), recorded temperatures of the shallow-water Badwater Lake over a period of about 2 weeks in April, 1993 (16.3–34.4 °C; Lowenstein et al., 1998), and mean annual ocean SST, which vary greatly with latitude (0–29.6 °C; Levitus, 2010). (B) The salinity estimates for the Messinian evaporites are consistent with marine salinity (gray bar is the 95% prediction interval for salinity estimates). For comparison, also shown are saturation salinities for gypsum and halite, and the range of salinities of the Infersa Saline Salt Pans in Sicily (103.1–236.3 psu; Turich et al., 2007), the modern Mediterranean Sea (13–28 psu; Levitus, 2010) and mean annual oceans, including areas with fresh water input (5.1–40.3 psu; Levitus, 2010). (For interpretation of the references to color in this figure, the reader is referred to the web version of this article.)

along the Rhone and Nile rivers. Clauzon (1982) estimates 1600 m of lowering based on a reconstruction of the paleo-channel of the Rhone River. Cross sections across the modern mouth of the Rhone (at Saintes Maries) show a buried channel incised to 1300 mbsl and backfilled by Early Pliocene marine sediments (see Figs. 4 and 5 in Clauzon, 1982). There is no information about when the bedrock valley was cut, or if it was cut in a subaerial setting, but the back filling by Pliocene marine sediments is taken as evidence that this channel was cut during a lowstand at some time during the Messinian salinity crisis (Clauzon, 1982). The commonly cited estimate of 1600 m of drawdown is based on extrapolation of the channel profile from Saintes Maries to the abyssal Mediterranean using an inferred gradient of 0.3%. In our opinion, direct observation of the bedrock depth from the Saintes Maries seismic survey provides the more useful constraint: that a lowstand of at least 1300 mbsl occurred at some time during the Miocene, assuming the canyon was cut in a subaerial setting. A similar incised channel is present at the mouth of the Nile River. Barber (1981) shows a seismic profile of a buried valley 100 km upstream of the mouth of the Nile River. The valley is cut 1400 m into Miocene sediments, and also backfilled by Early Pliocene marine sediments.

The argument of canyon incision is complicated by flexural deformation of the margins of the Mediterranean due to changing water and sediment loads (Norman and Chase, 1986; Govers et al., 2009). Modeling by Govers et al. (2009) shows that flexural isostasy due to deposition of the abyssal evaporites in a deep-water basin would have caused no more than 100 m of uplift at the mouth of the Rhone River. The elastic thickness of the lithosphere is thought to be significantly greater at the lower reach of the Nile River than below the mouth of the Rhone River. Govers et al. (2009) shows that several hundred meters of the observed valley incision in the Nile canyon is probably a result of flexural uplift caused by Messinian deposition in the deep Mediterranean. Given these observations, the Rhone canyon provides the better estimate for the drawdown during the Messinian salinity crisis to ~1300 mbsl, assuming subaerial canyon incision. Note that there is

no specific constraint on when during the Messinian this incision occurred.

An important issue, most recently addressed by Roveri et al. (2014b), is that these canyons could have been incised below sea level. Density underflows, whether driven by turbid mixtures of sediment or saline water, are able to erode their bed, as evidenced by submarine canyons and channels in the modern deep oceans. Roveri et al. (2014b) argue that the Rhone channel was deepened by energetic submarine flows of dense, hypersaline water. This scenario would require only 200 m of drawdown to create marginal basins where the dense brines could have been produced.

Ryan and Cita (1978) and Ryan (2009) call attention to widespread erosion on the upper slopes of the Mediterranean during the Messinian. They consider this evidence of subaerial exposure of the continental margins. However, Govers et al. (2009) shows that flexural uplift of the margins of the Mediterranean may have caused widespread erosion. In this interpretation, the marginal erosion occurred by submarine mass wasting.

4.4. Isostatic corrections

Our discussions above can be divided into five possible scenarios (Fig. 5, Table 2) for the amount of drawdown of the Mediterranean during the Messinian salinity crisis. These different scenarios cannot be directly compared until we account for the interrelationship between isostasy, drawdown, and water depth. The DSDP sites lie in the central part of the Mediterranean, far removed from the surrounding continental margins, so local isostasy (with no flexural modulation) can be used to estimate changes in depth associated with changing water and sediment loads (Norman and Chase, 1986; Govers et al., 2009). The core samples are currently at depth D_1 below modern sea level (Fig. 6). We estimate the depth D_0 and the water depth T_{w0} at the time of deposition of the uppermost abyssal evaporites. These deposits are currently overlain by layers of sediment and water with thicknesses T_{s1} and T_{w1} , and densities $\rho_s = 1900$ and $\rho_w = 1030$ kg/m³, respectively. At the end of the Messinian, the layer of overlying sediment $T_{s0} = 0$, and

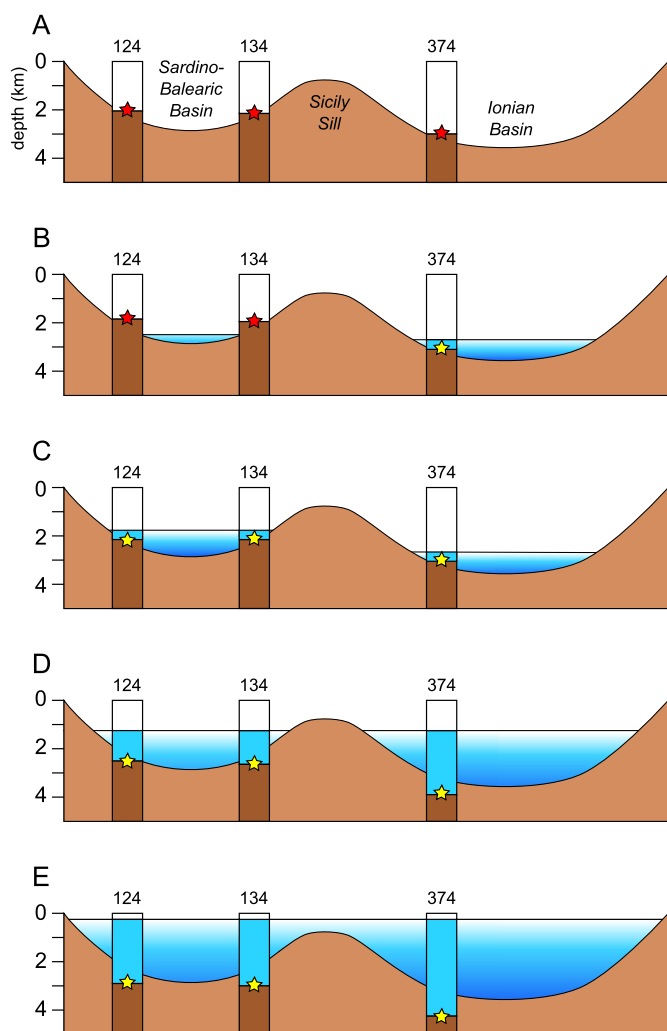


Fig. 5. Schematic diagram of the basin and water depths for the 5 scenarios discussed in the text. The vertical columns correspond to the isostatic balance used to calculate the depositional depth relative to modern sea level and water depth for each of the cores (see Fig. 6). Yellow and red stars indicate evaporite deposition in water depths that are consistent and inconsistent, respectively, with our geochemical results. (For interpretation of the references to color in this figure, the reader is referred to the web version of this article.)

is replaced by layers of water and air with thicknesses T_{w0} and T_{a0} . The thicknesses of the lower sediments, crust, and lithospheric mantle are held constant between the Messinian and present. This is an approximation given that the lower sediments might have compacted, but this effect is insignificant for our problem (Norman and Chase, 1986).

Case A shows zero water depth as predicted for complete evaporation (Hsü et al., 1973a, 1973b). The sea floor would have been 600–900 m shallower than modern due to the absence of a water load. Case B shows sea levels of 2515 and 2725 mbsl, as predicted for equilibrium basins in the western and eastern Mediterranean, respectively (Meijer and Krijgsman, 2005). For this case, the western drilling sites are subaerially exposed, lying ~600 m above sea level, which is inconsistent with our organic geochemical results. The eastern samples are at a water depth of 400 m, consistent with our findings. As noted above, the equilibrium level estimates by Meijer and Krijgsman (2005) are too large given that they do not account for influence of salinity on evaporation rate (Debenedetti, 1982; Salhotra et al., 1985). A shallower equilibrium level, by about 700 m, would be entirely consistent with our results, which indicate deep water at the time of evaporite deposition. Case C illus-

Table 2
Sea floor and water depths for abyssal Messinian evaporites.

Site	Case A			Case B			Case C			Case D			Case E		
	T_{w1} Present water depth (m)	T_{s1} Present sed. depth (m)	D_0 Sea floor elev. (mbsl)	T_{w0} Messinian water depth (m)											
124	2726	411	2063	0	2124	200	2403	1103	2893	2693	2893	2693	2893	2693	
134	2864	362	2137	0	2199	200	2510	1210	3000	2800	3000	2800	3000	2800	
374	4088	418	3008	409	3069	200	3769	2469	4259	4059	4259	4059	4259	4059	

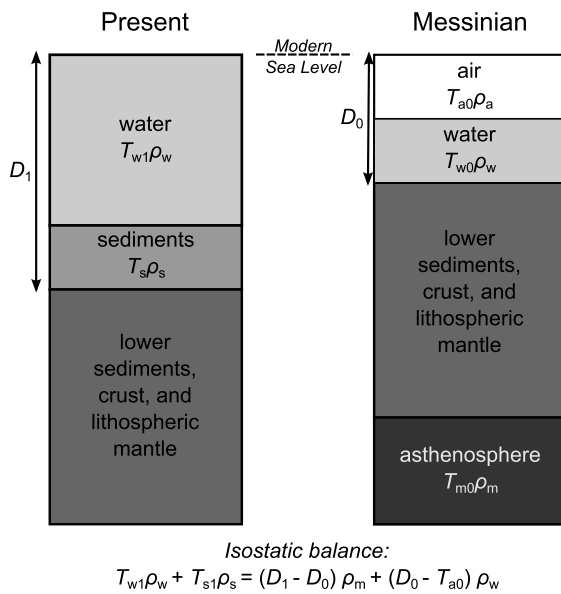


Fig. 6. Isostatic balance used to calculate the emplacement depth relative to modern sea level for the Messinian samples (D_0) and water depth during the Messinian (T_{w0}) after backstripping overlying water and sediment.

trates a ~ 200 m deep basin, which is the minimum required by our study. This estimate accounts, in an approximate way, for a mixed layer and an underlying brine at gypsum and halite saturation. In this case, sea level is lowered by ~ 2000 m and ~ 2900 m in the western and eastern basins, respectively. *Case D* shows a deep-water basin with a sea level of 1300 mbsl, consistent with subaerial incision of the Nile and Rhone rivers (Barber, 1981; Clauzon, 1982). *Case E* shows a deep-water basin with a sea level of 200 mbsl, as predicted by Roveri et al. (2014b) for submarine incision and erosion of the marginal Mediterranean.

Our geochemical results are consistent with any of Cases C, D or E. Note that this is not an exhaustive list of possible scenarios for the Messinian salinity crisis, or the only sea level scenarios constrained by our geochemical results. For example, our new evidence is in agreement with a scenario in which the Mediterranean sea level remained steady and fully connected to the Atlantic ocean, provided there was a mechanism to create a surface mixed layer and an underlying brine at gypsum and halite saturation. Our results do clearly rule out a scenario in which the evaporites analyzed in this study were deposited in a fully evaporated setting.

5. Conclusions

The organic compounds present in the abyssal Messinian evaporites clearly preclude the shallow-water hypothesis for deposition of the uppermost abyssal deposits. Evidence from marginal Mediterranean features, while highly debated, requires drawdown of no more than 1300 m during the Messinian, resulting in basin water depths of ~ 1200 m. The full story of the Messinian salinity crisis cannot be resolved until there is full sampling of the Messinian section beneath the abyssal Mediterranean sea floor. Our results highlight the ability of organic geochemistry, using modern chromatographic and mass spectrometry methods, to resolve the paleoenvironment of these ancient evaporites.

Acknowledgements

We thank Charlotte Schreiber, and Srinath Krishnan for productive discussions and suggestions. James Super, and Ellen Thomas provided help with analysis of the data. We are grateful for the use

of Mark Pagani's lab at Yale University. We also thank three anonymous reviewers for their thoughtful and thorough comments. This research used samples provided by the Integrated Ocean Drilling Program Core Repository at the University of Bremen. Elizabeth Christeleit acknowledges support from an NSF Graduate Fellowship and from Yale University.

References

- Barber, P.M., 1981. Messinian subaerial erosion of the proto-Nile Delta. *Mar. Geol.* 44, 253–272.
- Birgel, D., Guido, A., Liu, X., Hinrichs, K.U., Gier, S., Peckmann, J., 2014. Hypersaline conditions during deposition of the Calcare di Base revealed from archaeal di- and tetraether inventories. *Org. Geochem.* 77, 11–20.
- Blanc, P.L., 2006. Improved modeling of the Messinian Salinity Crisis and conceptual implications. *Palaeogeogr. Palaeoclimatol. Palaeoecol.* 238, 349–372.
- Brainerd, K.E., Gregg, M.C., 1995. Surface mixed and mixing depths. *Deep-Sea Res., Part 1, Oceanogr. Res. Pap.* 42, 1521–1543.
- Brongersma-Sanders, M., 1971. Origin of major cyclicity of evaporites and bituminous rocks: an actualistic model. *Mar. Geol.* 11, 123–144.
- Clauzon, G., 1982. Le canyon messinien du Rhone; une preuve decisive du "desiccated deep-basin model". In: Hsü, K.J., Cita, M.B., Ryan, W.B.F. (Eds.), *Bulletin de la Société Géologique de France*, vol. 3, pp. 597–610.
- Crosman, E.T., Horel, J.D., 2009. MODIS-derived surface temperature of the Great Salt Lake. *Remote Sens. Environ.* 113, 73–81.
- Debenedetti, A., 1982. The problem of the origin of the salt deposits in the Mediterranean and of their relations to the other salt occurrences in the Neogene formations of the contiguous regions. *Mar. Geol.* 49, 91–114.
- Dietz, R.S., 1963. Wave-base, marine profile of equilibrium, and wave-built terraces: a critical appraisal. *Geol. Soc. Am. Bull.* 74, 971–990.
- Gertman, I., Hecht, A., 2002. The Dead Sea hydrography from 1992 to 2000. *J. Mar. Syst.* 35, 169–181.
- Govers, R., Meijer, P., Krijgsman, W., 2009. Regional isostatic response to Messinian Salinity Crisis events. *Tectonophysics* 463, 109–129.
- Hardie, L.A., Lowenstein, T.K., 2004. Did the Mediterranean Sea dry out during the Miocene? A reassessment of the evaporite evidence from DSDP Legs 13 and 42A cores. *J. Sediment. Res.* 74, 453–461.
- Hopmans, E.C., Weijers, J.W., Schefuß, E., Herfort, L., Sinninghe Damsté, J.S., Schouten, S., 2004. A novel proxy for terrestrial organic matter in sediments based on branched and isoprenoid tetraether lipids. *Earth Planet. Sci. Lett.* 224, 107–116.
- Houpert, L., Testor, P., de Madron, X.D., Somot, S., D'Ortenzio, F., Estournel, C., Lavi-gne, H., 2015. Seasonal cycle of the mixed layer, the seasonal thermocline and the upper-ocean heat storage rate in the Mediterranean Sea derived from observations. *Prog. Oceanogr.* 132, 333–352.
- Hsü, K.J., 1972. Origin of Saline Giants: a critical review after the discovery of the Mediterranean evaporite. *Earth-Sci. Rev.* 8, 371–396.
- Hsü, K.J., Cita, M.B., Ryan, W.B.F., 1973a. The origin of the Mediterranean evaporite. In: Ryan, W.B.F., et al. (Eds.), *Initial Reports of the Deep Sea Drilling Project*, vol. 13, Part 4. U.S. Government Printing Office, Washington, DC, pp. 1203–1231.
- Hsü, K.J., Ryan, W.B.F., Cita, M.B., 1973b. Late Miocene desiccation of the Mediterranean. *Nature* 242, 240–244.
- Hsü, K.J., Ryan, W.B.F., Schreiber, B.C., 1973c. Petrography of a halite sample from Hole 134 – Balearic abyssal plain. In: Ryan, W.B.F., et al. (Eds.), *Initial Reports of the Deep Sea Drilling Project*, vol. 13, Part 2. U.S. Government Printing Office, Washington, DC, pp. 708–711.
- Hsü, K.J., Montadert, L., Bernoulli, D., Bizon, G., Cita, M.B., Erickson, A.J., Fabricius, F.H., Garrison, R.E., Kidd, R.B., Mèlierés, F., Mueller, C., Wright, R.C., 1978. Messina Abyssal Plain, Site 374. In: Hsü, K.J. (Ed.), *Initial Reports of the Deep Sea Drilling Project*, vol. 42. Texas A & M University, Ocean Drilling Program, College Station, TX, pp. 175–217.
- Karner, M., DeLong, E.F., Karl, D.M., 2001. Archaeal dominance in the mesopelagic zone of the Pacific Ocean. *Nature* 409, 507–510.
- Kim, J.H., van der Meer, J., Schouten, S., Helmke, P., Willmott, V., Sangiorgi, F., Koc, N., Hopmans, E.C., Sinninghe Damsté, J.S., 2010. New indices and calibrations derived from the distribution of crenarchaeal isoprenoid tetraether lipids: implications for past sea surface temperature reconstructions. *Geochim. Cosmochim. Acta* 74, 4639–4654.
- Krijgsman, W., Hilgen, F.J., Raffi, I., Sierro, F.J., Wilson, D.S., 1999. Chronology, causes and progression of the Messinian salinity crisis. *Nature* 400, 652–655.
- Levitus, S., 2010. *World Ocean Atlas 2009*. U.S. Gov. Printing Office, Washington, DC.
- Liu, Z., Pagani, M., Zinniker, D., DeConto, R., Huber, M., Brinkhuis, H., Shah, S.R., Leckie, R.M., Pearson, A., 2009. Global cooling during the Eocene-Oligocene climate transition. *Science* 323, 1187–1190.
- Lofi, J., Sage, F., Déverchère, J., Loncke, L., Maillard, A., Gaullier, V., Thion, I., Gillet, H., Guennoc, P., Gorini, C., 2011. Refining our knowledge of the Messinian salinity crisis records in the offshore domain through multi-site seismic analysis. *Bull. Soc. Géol. Fr.* 182, 163–180.

- Lowenstein, T.K., Li, J., Brown, C.B., 1998. Paleotemperatures from fluid inclusions in halite: method verification and a 100,000 year paleotemperature record, Death Valley, CA. *Chem. Geol.* 150, 223–245.
- Manzi, V., Gennari, R., Hilgen, F., Krijgsman, W., Lugli, S., Roveri, M., Sierro, F.J., 2013. Age refinement of the Messinian salinity crisis onset in the Mediterranean. *Terra Nova* 25, 315–322.
- Mark, D.M., Church, M., 1977. On the misuse of regression in Earth science. *J. Int. Assoc. Math. Geol.* 9, 63–75.
- Meijer, P.T., Krijgsman, W., 2005. A quantitative analysis of the desiccation and refilling of the Mediterranean during the Messinian Salinity Crisis. *Earth Planet. Sci. Lett.* 240, 510–520.
- Mottura, S., 1872. Sulla formazione terziaria nella zona solfifera della Sicilia. *Topografia di G. Barbèra*.
- Norman, S.E., Chase, C.G., 1986. Uplift of the shores of the western Mediterranean due to Messinian desiccation and flexural isostasy. *Nature* 322, 450–451.
- Ogniben, L., 1957. Petrografia della Serie Solfifera Siciliana e considerazioni geologiche relative. Servizio geologico d'Italia.
- Osborne, C., 1991. Statistical calibration: a review. *Int. Stat. Rev.* 59, 309–336.
- Pearson, A., Ingalls, A.E., 2013. Assessing the use of archaeal lipids as marine environmental proxies. *Annu. Rev. Earth Planet. Sci.* 41, 359–384.
- Roveri, M., Flecker, R., Krijgsman, W., Lofi, J., Lugli, S., Manzi, V., Sierro, F.J., Bertini, A., Camerlenghi, A., De Lange, G., Govers, R., Hilgen, F.J., Hübscher, C., Meijer, P.T., Stoica, M., 2014a. The Messinian Salinity Crisis: past and future of a great challenge for marine sciences. *Mar. Geol.* 352, 25–58.
- Roveri, M., Manzi, V., Bergamasco, A., Falcieri, F.M., Gennari, R., Lugli, S., Schreiber, B.C., 2014b. Dense shelf water cascading and Messinian Canyons: a new scenario for the Mediterranean salinity crisis. *Am. J. Sci.* 314, 751–784.
- Roveri, M., Lugli, S., Manzi, V., Gennari, R., Schreiber, B.C., 2014c. High-resolution strontium isotope stratigraphy of the Messinian deep Mediterranean basins: implications for marginal to central basin correlation. *Mar. Geol.* 349, 113–125.
- Ryan, W.B.F., 2009. Decoding the Mediterranean salinity crisis. *Sedimentology* 56, 95–136.
- Ryan, W.B.F., Cita, M.B., 1978. The nature and distribution of the erosional surfaces-indicators of a several-kilometer-deep Mediterranean in the Miocene. *Mar. Geol.* 27, 193–230.
- Ryan, W.B.F., Hsü, K.J., Cita, M.B., Dumitrica, P., Lort, P., Maync, W., Nesteroff, W.D., Pautot, P., Stradner, H., Wezel, F.C., 1973a. Balaric Rise – Site 124. In: Ryan, W.B.F., Hsü, K.J. (Eds.), *Initial Reports of the Deep Sea Drilling Project*, vol. 13, Part 1. U.S. Government Printing Office, Washington, DC, pp. 133–174.
- Ryan, W.B.F., Hsü, K.J., Cita, M.B., Dumitrica, P., Lort, P., Maync, W., Nesteroff, W.D., Pautot, P., Stradner, H., Wezel, F.C., 1973b. Boundary of Sardinia Slope with Balearic Abyssal Plain – Sites 133 and 134. In: Ryan, W.B.F., Hsü, K.J. (Eds.), *Initial Reports of the Deep Sea Drilling Project*, vol. 13, Part 1. U.S. Government Printing Office, Washington, DC, pp. 465–514.
- Salhotra, A.M., Adams, E.E., Harleman, R.F., 1985. Effect of salinity and ionic composition on evaporation: analysis of Dead Sea evaporation pans. *Water Resour. Res.* 21, 1336–1344.
- Schmalz, R.F., 1969. Deep-water evaporite deposition, a genetic model. *Am. Assoc. Pet. Geol. Bull.* 53, 798–823.
- Schmalz, R.F., 1991. The Mediterranean Salinity Crisis: alternative hypothesis. *Carb. Evap.* 6, 121–126.
- Schouten, S., Hopmans, E.C., Schefuß, E., Sinninghe Damsté, J.S., 2002. Distributional variations in marine crenarchaeotal membrane lipids: a new organic proxy for reconstructing ancient sea water temperatures? *Earth Planet. Sci. Lett.* 204, 265–274.
- Schouten, S., Huguet, C., Hopmans, E.C., Kienhuis, M.V., Sinninghe Damsté, J.S., 2007. Analytical methodology for TEX₈₆ paleothermometry by high-performance liquid chromatography/atmospheric pressure chemical ionization-mass spectrometry. *Anal. Chem.* 79, 2940–2944.
- Schouten, S., Hopmans, E.C., Sinninghe Damsté, J.S., 2013. The organic geochemistry of glycerol dialkyl glycerol tetraether lipids: a review. *Org. Geochem.* 54, 19–61.
- Schreiber, B.C., El Tabakh, M., 2000. Deposition and early alteration of evaporites. *Sedimentology* 47, 215–238.
- Sinninghe Damsté, J.S., Schouten, S., Hopmans, E.C., van Duin, A.C., Geenevasen, J.A., 2002. Crenarchaeol the characteristic core glycerol dibiphytanyl glycerol tetraether membrane lipid of cosmopolitan pelagic crenarchaeota. *J. Lipid Res.* 43, 1641–1651.
- Sonnenfeld, P., 1985. Models of Upper Miocene evaporite genesis in the Mediterranean region. In: Stanley, D.J., Wezel, F. (Eds.), *Geological Evolution of the Mediterranean Basin*. Springer, New York, pp. 323–346.
- Thomas, E., 2015. **Written communication.**
- Topper, R.P.M., Meijer, P.T., 2013. A modeling perspective on spatial and temporal variations in Messinian evaporite deposits. *Mar. Geol.* 336, 44–60.
- Trommer, G., Siccha, M., van der Meer, M.T.J., Schouten, S., Sinninghe Damsté, J.S., Schulz, H., Hemleben, C., Kucera, M., 2009. Distribution of Crenarchaeota tetraether membrane lipids in surface sediments from the Red Sea. *Org. Geochem.* 40, 724–731.
- Turich, C., Freeman, K.H., Bruns, M.A., Conte, M., Jones, A.D., Wakeham, S.G., 2007. Lipids of marine Archaea: patterns and provenance in the water-column and sediments. *Geochim. Cosmochim. Acta* 71, 3272–3291.
- Turich, C., Freeman, K.H., 2011. Archaeal lipids record paleosalinity in hypersaline systems. *Org. Geochem.* 42, 1147–1157.
- Wang, H., Liu, W., Zhang, C.L., Jiang, H., Dong, H., Lu, H., Wang, J., 2013. Assessing the ratio of archaeol to caldarchaeol as a salinity proxy in highland lakes on the northeastern Qinghai–Tibetan Plateau. *Org. Geochem.* 54, 69–77.
- Wuchter, C., Schouten, S., Coolen, M.J.L., Sinninghe Damsté, J.S., 2004. Temperature dependent variation in the distribution of tetraether membrane lipids of marine crenarchaeota: implications for TEX₈₆ paleothermometry. *Paleoceanography* 19, 4028.